Effect of Hydrodynamic Interactions on DNA Dynamics in Extensional Flow: Simulation and Single Molecule Experiment

Charles M. Schroeder,[†] Eric S. G. Shaqfeh,*,[‡] and Steven Chu[§]

Department of Chemical Engineering, Stanford University, Stanford, California 94305; Departments of Chemical and Mechanical Engineering, Stanford University, Stanford, California 94305; and Departments of Physics and Applied Physics, Stanford University, Stanford, California 94305

ABSTRACT: Intramolecular hydrodynamic interactions (HI) in flexible polymer chains influence both the equilibrium and nonequilibrium physical properties of macromoecules. In this work, we utilize a combination of single molecule experimental techniques and Brownian dynamics (BD) simulation to investigate the role of HI and excluded-volume (EV) interactions for DNA molecules ranging in contour length from 150 to 1300 μm. Epifluorescence microscopy is used to directly observe the dynamics of DNA molecules in planar extensional flow, and a semiimplicit bead−spring BD algorithm with fluctuating HI and EV interactions is presented. Quantitatitative agreement between ensemble average transient molecular extension in experiment and BD simulation is shown for DNA with 150 μm contour length. Simulations show polymer conformation hysteresis for larger DNA chains (1300 μm in length) when HI and EV parameters are chosen such that simulation results match the experimental polymer relaxation time and polymer stretch at flow strengths below the coil−stretch transition. Furthermore, conformation-dependent resistivities are extracted from BD simulation for DNA chains 1300 μm in length, and this drag functionality is utilized in a coarse-grained Brownian dumbbell model with variable resistivity. Finally, steady-state molecular extension results from the coarse-grained model are compared to simple polymer kinetic theory for a dumbbell with variable resistivity.

1. Introduction

The nonequilibrium behavior of flexible polymer molecules in flows of dilute solutions is complex, and an accurate description of the dynamics of long-chain macromolecules can be a daunting task. Traditionally, bulk rheological experiments including flow bire-fringence[1−3] and light scattering measurements[4,5] were used to infer information regarding polymer conformation, orientation, and chain stretch in strong flows. More recently, the advent of single molecule visualizations using fluorescence microscopy has allowed for the direct observation of individual DNA molecules in flows of dilute solutions in shear,[6] planar extensional,[7,8] and general two-dimensional mixed flows.[9] Experimental results from these studies have elucidated complex polymer behavior in a number of ways. First, studies of DNA allow for observation of well-characterized, monodisperse polymer chains of known contour length,[10] with equilibrium properties such as chain diffusivity[11] and polymer relaxation times known within small degrees of experimental uncertainty. Furthermore, observation of transient molecular stretch reveals rich individualistic molecular behavior with regard to chain configuration.[7] Dilute solution studies involving DNA are performed at extremely low concentrations ($\approx 10^{-5}c^*$, where c^* is the polymer overlap concentration) such that interpolymer interactions are absent and cause no flow-induced changes to a well-defined, spatially homogeneous flow field. Results including transient and steady chain stretch in flow have allowed for significant progress to be made in areas of model development and simulation algorithm testing. Model parameters may be chosen such that the simulation accurately captures known properties of DNA molecules, and the nonequilibrium microstructual information between experiment and simulation may be directly compared. A careful coupling of single molecule visualization and Brownian dynamics simulation of polymer chains provides a powerful combination of tools to study the dynamics of polymer chains in flow.

Many previous Brownian dynamics simulations of bead−spring and bead−rod models for lambda DNA chains have included the assumption that polymer chains are free-draining,[12−14] albeit the authors calculate bead drag coefficients to match the longest polymer relaxtion time measured from experiment. As discussed below, such models for lambda DNA show quantitative agreement with dynamical polymer behavior determined from single molecule experiments. In a free-draining bead−spring polymer model, all of the beads move through the solvent without inducing perturbations to the solvent velocity.[15] However, in a realistic polymer chain, portions of the polymer disturb the solvent flow field, and nearby regions of the molecule are affected by these hydrodynamic interactions (HI). In the coiled state, interior monomer units are shielded from the full solvent velocity by outer portions of the molecule. However, in the fully extended conformation, monomer units are more exposed to the flow, and the effects of HI are diminished. In this state, the fluid exerts a more effective frictional grip on the polymer molecule.

Hydrodynamic interactions have well-known effects on the linear viscoelastic (LVE) properties of polymers.[16,17] The longest polymer relaxtion time τ scales as molecular weight M like $\tau \sim M^{1.5}$ for HI-dominant

---

[†] Department of Chemical Engineering.
[‡] Departments of Chemical and Mechanical Engineering.
[§] Departments of Physics and Applied Physics.
* To whom correspondence should be addressed. E-mail: eric@chemeng.stanford.edu.

polymers in a Θ solvent and $\tau \sim M^{1.8}$ for polymer chains in a good solvent, compared to $\tau \sim M^2$ for free-draining chains.[16] Furthermore, the storage and loss moduli from oscillatory LVE measurements scale with frequency ω as $\omega^{2/3}$ rather than $\omega^{1/2}$ in the intermediate frequency regime for polymers in Θ solvents.[16] As pointed out by Hsieh et al.,[17] inclusion of HI is required even for an accurate qualitative description of the linear rheological behavior of dilute solutions of macromolecules.

In addition to Brownian dynamics (BD) simulation of free-draining polymer models, several recent studies have also focused on the effects of intrachain HI and excluded volume on polymer dynamics in extensional flow. Cifre and de la Torre[18] examined the dilute solution behavior of flexible polymers in steady uniaxial extensional flow using BD simulation of bead−spring chains with HI and excluded-volume (EV) interactions. In an additional study, Cifre and de la Torre[19] investigated the rate of polymer coil unraveling in transient extensional flows using BD simulation of bead−spring chains with HI and EV. Employing a bead−rod model with intramolecular HI and EV, Neelov et al.[20] simulated the behavior of linear polymers in extensional flow using BD simulation. In this work, the authors determine a molecular weight scaling for the critical extensional flow rate at which the molecules exhibit the coil−stretch transition in extensional flow. Neelov and Adolf[21] extended this original work for linear polymers to dendrimers in uniaxial extensional flow, again using a bead−rod model with intramolecular HI and excluded-volume interactions.

The effects of HI on the nonequilibrium dynamics of polymer molecules have been previously studied using kinetic theory. Zimm[22] represented bead disturbances to the solvent flow field as point forces (Stokeslets). For viscous dominated (low Reynolds number) flows, a velocity disturbance $\mathbf{v}'(\mathbf{r}')$ at a location $\mathbf{r}'$ is linearly proportional to the disturbance force $\mathbf{F}$ that a neighboring bead at location $\mathbf{r}$ exerts on the solvent, giving $\mathbf{v}'(\mathbf{r}') = \mathbf{G} \cdot \mathbf{F}(\mathbf{r})$, where $\mathbf{G}$ is the Green's function of the time-independent, linear Navier−Stokes equation. Inclusion of these interactions into polymer kinetic theory yields nonlinear equations for the moments of the polymer end-to-end vector, even for chains with a linear Hookean force law. Because the motion of the polymer would depend on its instantaneous configuration, Zimm linearized the problem and was able to make analytical progress by replacing $\mathbf{G}$ by its ensembled-averaged property at equilibrium. This process yields a model with the correct (HI-dominant) molecular weight scaling laws for diffusivity and polymer relaxation time but fails to describe polymer dynamics in nonequilibrium flow conditions. A refinement this "preaveraging approximation" involves averaging the HI tensors in the proper flow field. This so-called "consistent averaging model"[23] is successful in predicting a shear thinning viscosity (η_p) and a nonvanishing (although positive at low shear rates) second normal stress coefficient (Ψ_2) in simple shear flow.[24] However, this method ignores fluctuations in HI because it inherently involves an HI interaction tensor averaged over all configuations. Significant progress was made by Öttinger[25,24] and independently by Wedgewood[26] by assuming Gaussian distribution functions which leads to a closed set of equations for the ensemble-averaged second moment of the end-to-end vectors for bead−spring chains. This model gives good agreement with results from Brownian dynamics

simulation for both η_p and Ψ_2 for Hookean dumbbells in shear flow. In addition to kinetic theory, Brownian dynamics simulation allows for solution of the equations of motion for the beads (without approximations) for large polymer chains with fluctuating HI.

It has generally been believed that polymers with many persistence lengths should exhibit significant intramolecular hydrodynamic interactions. In this regard, it is surprising that the free-draining model accurately captures the dynamical flow behavior of lambda DNA as shown in previous studies.[12−14] Recent work[27] showed that inclusion of hydrodynamic interactions and excluded volume (EV) into a bead−spring polymer model gave neither a qualitative nor an appriciable quantitive change in the transient or steady molecular extension of lambda DNA in shear and planar extensional flow. Lambda DNA is an unusual polymer in the following sense: it is large enough to exhibit non-free-draining behavior at equilibrium (for example, chain diffusivity scales as molecular weight $M^{-0.6}$ in a good solvent[11]), yet sufficiently small such that inclusion of conformation-dependent drag is essentially unnecessary for a quantitative description of transient and steady dynamics in shear or planar extensional flow. Hsieh et al.[17] also reach this conclusion regarding lambda DNA using Brownian dynamics simulations with fluctuating HI without excluded-volume interactions. Other experimental evidence also illustrates the unusual dynamical behavior of lambda DNA. The fluctuating motion of partially extended single lambda DNA molecules can be described by eight linearly independent normal modes.[28] However, the modal relaxation times exhibit a Zimm-like scaling, suggesting that HI effects should be considered at moderate polymer extensions. For slightly larger DNA molecules approximately 4 lambda (126 μm) in length, simulations of Jendrejack et al.[27] show that inclusion of HI slightly alters the transient molecular response in planar extensional flow.

Recent experimental work by Schroeder et al.[29] shows that extremely large chains of DNA ($L \approx 1.3$ mm, equivalent to $\approx 20\,000$ persistence lengths) were required to observe conformational hysteresis. On the basis of the results from this study, it is clear that HI can affect the nonlinear rheology of flexible polymers in a qualitatively different manner than previously expected.[16] Conformation hysteresis and, more generally, conformation-dependent drag may have a profound impact on the development of constitutive equations for polymer solutions and may be required for accurate modeling of turbulent drag reduction.[30,31] Therefore, it behooves us to carefully study the effects of HI on polymer chain dynamics by taking advantage of nonequilibrium microstructural data from both single molecule experimental techniques and Brownian dynamics simulation.

2. Experimental Section

2.1. Apparatus. Polymer molecules were imaged near the stagnation point of a planar extensional flow in a novel cross-slot apparatus. The flow device[32] was used in recent work regarding polymer conformation hysteresis[29] and is unique in that it allows for extremely long observation times of polymers in a planar extensional flow. The apparatus consists of a quartz microscope slide (1 in. × 3 in. × 1 mm) with four holes drilled such that a cross pattern was formed by the channels. A single piece of Parafilm onto which a cross shape has been fashioned with a razor blade was sandwiched between the clean slide

and a glass coverslip (no. 1, 24 × 60 mm). The construction was gently heated for ≈1 min on a hot plate, resulting a sealed flow device with ≈6−7 mm wide and ≈150 μm deep channels. The flow cell was affixed on a custom-built aluminum mount, and microbore flow lines (0.04 in. i.d., Upchurch) were seated against the underside of the cell with small O-rings between the ends of the flow tubing and channel openings. The entire flow cell mount was then fastened to a microscope stage. Both outlet flow lines drained into separate waste containers open to the atmosphere. Feedback control of the stagnation point location and hence molecule trapping was achieved by varying the vertical height of one waste container relative to the other. This action varied the hydrostatic pressure head at one submerged waste tube outlet with respect to the other and enabled sensitive adjustment of the stagnation point position.[32,29] Molecules were imaged near the stagnation point (where the flow type was shown to be purely extensional[29]) and away from the autofluorescent channel walls of the cell. Finally, molecules were imaged near the center plane of the flow cell at depths of 60 ± 10 μm where only small variations in the calibrated fluid strain rates $\dot{\epsilon}$ occur.

2.2. Materials. Concatemers of lambda DNA (New England Biolabs) ranging in size from 1-mers to ≈20-mers were purchased in 1% LMP agarose gel. Lambda DNA concatemers (≈0.01 μg/μL) embedded in gel were incubated for 24 h in the presence of T4 DNA ligase (NEB) and ligase buffer to complete phosphodiester bonds along the DNA backbone. DNA was extracted from agarose by melting the gel with gentle heating at 65 °C for 10 min, followed by staining at DNA concentrations ≈2 × 10⁻⁴ μg/μL in the presence of ≈10⁻⁷ M YOYO-1 fluorescent dye (Molecular Probes) for ≈1 h. We attempted to maintain the ratio of dye molecules to nucleic acid base pairs near 1:4 as in previous single molecule studies of lambda phage DNA.[6] YOYO-1 dye was used to stain DNA in all experiments except those involving 1300 μm DNA (as described in previous work[29]) and steady-state molecular extension experiments involving 7-lambda DNA; in these two cases, Sytox Green dye (Molecular Probes) was used to fluorescently label DNA.

We used the above gel procedure to extract lambda DNA concatemers 7-lambda in length. DNA with contour lengths (*L*) around 340 μm was obtained both from the above procedures and from *Escherichia coli* DNA, a generous gift from US Genomics. Concentrations of DNA in the observation buffers were extremely dilute ($c \approx 10^{-5}c^*$) to prevent intermolecular interactions. For transient extensional flow data, DNA were imaged in a pH 8.0 aqueous buffer containing 10 mM tris-HCl, 10 mM NaCl, and 2 mM EDTA. Photobleaching of the dye was substantially slowed (by a factor of ≈50, depending on the choice of dye) by adding enzymatic oxygen scavenging reagents consisting of 0.3% (v/v) glucose, glucose oxidase (0.05 μg/μL), and catalase (0.01 μg/μL). Addition of 1% (v/v) β-mercaptoethanol also helped to prevent photobleaching of the dye by removing oxygen radicals from solution. Solutions contained 45% (w/w) or 0% (w/w) sucrose for 7-lambda (*L* = 150 μm) and 340 μm DNA, respectively, to control buffer viscosities. Experiments involving DNA relaxation from high stretch were performed in a aqueous buffer containing 60% (w/w) sucrose and 1% (w/w) glucose and otherwise with the same conditions as described above. Aqueous buffers were filtered through 0.2 μm filters (Millipore) to remove particulate impurities before addition of DNA and oxygen scavenging agents.

2.3. General Procedures. An upright Zeiss Axioplan microscope with an infinite focal length objective lens was used in epifluorescence. When imaging 7-lambda DNA concatemers, a Nikon 60×, 1.2 numerical aperture (NA) water immersion objective lens was used. For the 340 μm contour length DNA data, an Olympus 40×, 1.0 NA oil immersion objective lens was used. All experiments were performed with a demagnifying lens (0.31×) inserted between the microscope and CCD camera to provide a wider field of view. We imaged DNA with a back-illuminated Micromax 512BFT CCD camera (Roper Scientific). Light from a 100 W mercury lamp passed through a 470 ± 20 nm band-pass absorption filter (Chroma) and was used to illuminate the sample. Emitted fluorescent light passed through a 505 nm long-pass dichroic filter and a band-pass

emission filter (535 ± 25 nm) and was directed to the CCD detector. To minimize photobleaching of the dye, we used a mechanical shutter (Uniblitz) for experiments involving 340 μm long DNA such that each molecule was imaged with a ¹/₃ illumination cycle. Airtight glass syringes (Hamilton) were gently filled with dilute solutions of fluorescent DNA, as described in section 2.2. Fluid was injected into the flow chamber by driving the syringe with an encoded feedback controlled motor (Maxon) that provided small fluctuations in solvent velocity as quantified by bead tracking studies.[29]

The feedback-controlled stagnation point flow device allows for the imaging of DNA molecules for arbitrarily long observation times t_{obs} or accumulated fluid strains $\epsilon = \dot{\epsilon} t_{obs}$. By first flowing the fluid at high flow rates at which the polymers are stretched, we locate a DNA molecule of acceptable length and "trap" it near the stagnation point by varying the vertical height of one outlet waste container, as described in section 2.1. To be "trapped" in the flow device, the stretched DNA molecule merely needs to appear in the image area of the microscope and does not actually need to closely approach (for example, within a few microns) the stagnation point. Next, we measure its relaxation time by stretching the molecule at high flow rates, followed by tracking its extension after cessation of the flow. Relaxation times were calculated by tracking the projected image of polymer extension as a function of time and fitting the final 30% of the extension to a decaying exponential function $\langle x \cdot x \rangle = A \exp(-t/\tau) + B$, where τ is the longest polymer relaxation time and *A* and *B* are fitting constants. The average polymer relaxtion time τ for 7-lambda DNA in 8.4 cP sucrose buffer was 19.8 ± 0.5 s for a 56-molecule ensemble, and τ was found to be 11.0 ± 0.2 s for 340 μm DNA in 1.0 cP buffer (49-molecule ensemble). The buffer viscosity was adjusted to 49 cP for experiments involving the relaxation of 7-lambda DNA from large extensions. A dimensionless flow strength, the Deborah number ($De = \dot{\epsilon}\tau$), is defined as a ratio of the relevant polymer time scale τ to the characteristic fluid stretching time $(\dot{\epsilon})^{-1}$.

Generally, we measure the transient molecular extension of a single molecule several times. Between transient trajectory runs, we allow the molecule to relax to an equilibrium configuration (with no illumination) and wait several τ to ensure a completely random initial state. Although precautions are taken to minimize photobleaching of the intercalating fluorescent DNA dyes (see section 2.2), we generally only observe a single DNA molecule over the course of ≈5 transient trajectories to maintain constant polymer physical properties (such as τ). Movies of polymer extension were saved directly to the computer, and the molecular extension at each movie frame was analyzed by an intensity threshold algorithm and verified by eye.

3. Brownian Dynamics Simulation

3.1. Model Description. We employ a model for Brownian dynamics simulation of a system of *N* particles that are subject to interparticle forces and fluctuating hydrodynamic interactions as originally presented by Ermak and McCammon.[33] Although this model has broad applicability and may be implemented to simulate the behavior of (for example) colloidal particles, we use it in a bead−spring description of flexible polymer molecules in dilute solution flows. In general, two equivalent approaches are possible for an accurate quantitative description of the dynamics of a system of Brownian particles: solution of the phase space (configuration space) distribution of particle position via a Fokker−Planck equation or direct simulation of particle trajectories with a Langevin description of particle motion, from which the appropriate distribution functions may be calculated. We choose the Langevin description and model the dynamics of Brownian particles affected by thermal fluctuations of the solvent. We assume that the particle momenta relax to equilibrium

much faster than the particle configurations and focus on time scales longer than the momentum relaxation time. This assumption, common in Brownian dynamics simulations, is equivalent to assuming that the particle velocity distribution is Maxwellian about a mass-averaged solvent velocity.[34]

A statement of force balance for each bead i yields the Langevin equations for a system of N Brownian particles with interparticle forces and fluctuating HI:

$$m_i \, \dot{\mathbf{v}}_i = \sum_{j=1}^{N} \zeta_{ij} \cdot \left(\mathbf{v}_j - \frac{\mathrm{d}\mathbf{r}_j}{\mathrm{d}t} \right) + \mathbf{F}_i + \sqrt{2} \sum_{j=1}^{N} \boldsymbol{\sigma}_{ij} \cdot \mathbf{W}_j \quad (1)$$

where m_i is the mass of bead i, $\mathbf{v}_i$ is the solvent velocity at bead i, ζ_{ij} is the configuration-dependent resistance tensor, $\mathbf{r}_i$ is the position of bead i, and $\mathbf{F}_i$ is the net interparticle (entropic spring and excluded volume) force on bead i. The coefficient tensor $\boldsymbol{\sigma}_{ij}$ is related to the resistance tensor ζ_{ij} by the relation

$$\zeta_{ij} = \frac{1}{kT} \sum_{l=1}^{N} \boldsymbol{\sigma}_{il} \cdot \boldsymbol{\sigma}_{jl} \quad (2)$$

and $\mathbf{W}_i$ is a Wiener process[15] such that

$$\langle \mathbf{W}_i \rangle = 0 \quad (3)$$

$$\langle \mathbf{W}_i(t) \, \mathbf{W}_j(t') \rangle = \boldsymbol{\delta}_{ij} \delta(t - t') \approx \frac{\boldsymbol{\delta}_{ij}}{t - t'} \quad (4)$$

where $\boldsymbol{\delta}_{ij}$ is the second-order isotropic tensor and $\delta(t)$ is the Dirac delta function. The expression for the variance of $\mathbf{W}_i$ is representative of a Wiener process, and the coefficients are chosen to satisfy the fluctuation dissipation theorem.[35] The approximate form in eq 4 provides a discrete expression for the Brownian forces exerted during a time step $\mathrm{d}t = t - t'$.

Ignoring bead inertia, eq 1 can be manipulated to yield set of a stochastic differential equations for the positions of beads $i = 1$ to N:[33]

$$\mathrm{d}\mathbf{r}_i = \left(\kappa \cdot \mathbf{r}_i + \sum_{j=1}^{N} \frac{\partial}{\partial \mathbf{r}_j} \cdot \mathbf{D}_{ij} + \sum_{j=1}^{N} \frac{\mathbf{D}_{ij} \cdot \mathbf{F}_j}{kT} \right) \mathrm{d}t + \sqrt{2} \sum_{j=1}^{i} \boldsymbol{\alpha}_{ij} \cdot \mathrm{d}\mathbf{W}_j \quad (5)$$

where the Wiener process $\mathrm{d}\mathbf{W}_j$ is conveniently expressed as

$$\mathrm{d}\mathbf{W}_j = \sqrt{\mathrm{d}t} \mathbf{n}_j \quad (6)$$

where $\mathbf{n}_j$ is a randomly distributed Gaussian vector with zero mean and unit variance. We assume spatially homogeneous velocity fields such that the solvent velocity $\mathbf{v}(\mathbf{r})$ can be expressed as $\mathbf{v}(\mathbf{r}) = \kappa \cdot \mathbf{r}$, where κ is the (constant) velocity gradient tensor. In eq 5, $\mathbf{D}_{ij}$ is the mobility tensor and is related to ζ_{ij} by the relation $\sum_l \zeta_{il} \mathbf{D}_{lj} = kT \boldsymbol{\delta}_{ij}$. Finally, the mobility tensor $\mathbf{D}_{ij}$ is related to the coefficient tensor $\boldsymbol{\alpha}_{ij}$ by the relation

$$\mathbf{D}_{ij} = \sum_{l=1}^{N} \boldsymbol{\alpha}_{il} \cdot \boldsymbol{\alpha}_{jl} \quad (7)$$

There are many possible choices for the mobility tensor $\mathbf{D}_{ij}$, and we choose $\mathbf{D}_{ij}$ as the Rotne−Prager−Yamakawa (RPY) tensor,[36] which has been proven to be positive-semidefinite for all polymer chain configurations. The RPY tensor has the added advantage that terms in eq 5 involving its spatial gradients are exactly zero; this feature greatly simplifies computation calculations. It should be noted that the RPY tensor accounts for spherically symmetric bead−bead interactions, and perhaps a more rigorous model that incorporates distributed, anisotropic interactions along a polymer chain may be more appropriate for an accurate description of flexible polymer behavior.[22] Nevertheless, the RPY mobility tensor is given by

$$\mathbf{D}_{ij} = \frac{kT}{\zeta} \mathbf{I}_{ij} \quad \text{if } i = j \quad (8)$$

$$\mathbf{D}_{ij} = \frac{kT}{8\pi\eta r_{ij}} \left[\left(1 + \frac{2a^2}{3r_{ij}^2} \right) \mathbf{I}_{ij} + \left(1 - \frac{2a^2}{r_{ij}^2} \right) \frac{\mathbf{r}_{ij}\mathbf{r}_{ij}}{r_{ij}^2} \right]$$
$$\text{if } i \neq j \text{ and } r_{ij} \geq 2a \quad (9)$$

$$\mathbf{D}_{ij} = \frac{kT}{\zeta} \left[\left(1 - \frac{9r_{ij}}{32a} \right) \mathbf{I}_{ij} + \frac{3\mathbf{r}_{ij}\mathbf{r}_{ij}}{32ar_{ij}} \right]$$
$$\text{if } i \neq j \text{ and } r_{ij} < 2a \quad (10)$$

where a is the bead radius, $\mathbf{r}_{ij}$ is the vector between beads i and j, and $r_{ij} = |\mathbf{r}_{ij}|$. The quantity h^* is often defined as the hydrodynamic interaction parameter in HI studies such that

$$h^* = a \sqrt{\frac{H}{\pi kT}} \quad (11)$$

The Hookean spring constant H is given by $H = 3kT/ N_{k,s}b_k^2$. The quantity h^* in eq 11 is the approximate ratio of the bead radius to the equilibrium extension of a spring; we therefore anticipate physically reasonable values of h^* to be less than $\approx 1/2$.[15] It should be noted that the quantity h^* arises naturally as a collection of constants that appears in an expression for the pre-averaged Oseen tensor. Therefore, h^* and the bead radius a are related quantities and should not be chosen separately.

We nondimensionalize eq 5 with an appropriate length scale (l_s) and time scale (t_s) such that $t_s = \zeta/4H$ and $l_s = \sqrt{kT/H}$, where ζ is the bead resistivity.[37] In this model, each spring is finitely extensible and represents only a portion of the entire polymer molecule, where the number of Kuhn steps per spring is denoted as $N_{k,s}$. The total number of Kuhn segments $N_{k,tot}$ in the molecule is $N_{k,tot} = (N - 1)N_{k,s}$, the Kuhn step size is b_k, and the total dimensional contour length L of the macromolecule is $L = N_{k,tot}b_k$. The spring connector vector for spring i can be defined as $\mathbf{Q}_i = \mathbf{r}_{i+1} - \mathbf{r}_i$. We now recast the eq 5 in terms of the spring connector vectors in dimensionless form as

$$\mathrm{d}\mathbf{Q}_i = [Pe(\kappa \cdot \mathbf{Q}_i) + \sum_{j=1}^{N} (\mathbf{D}_{i+1,j} - \mathbf{D}_{i,j}) \cdot (\mathbf{F}_j^E + \mathbf{F}_j^{EV})] \, \mathrm{d}t +$$
$$\sqrt{2} \sum_{j=1}^{i} (\boldsymbol{\alpha}_{i+1,j} - \boldsymbol{\alpha}_{i,j}) \cdot \mathrm{d}\mathbf{W}_j \quad (12)$$

where the subscripts on vector $\mathbf{Q}$ refer to spring vectors such that $1 \leq i \leq N - 1$, $\mathbf{F}_i^E$ is the net entropic spring force exerted on bead i, $\mathbf{F}_i^{EV}$ is the net excluded-volume force on bead i, and Pe is the bead Péclet number such that

that $Pe = \dot{\epsilon}\zeta/4H$. The total entropic force on bead i is given by

$$\mathbf{F}_i^{\mathrm{E}} = \begin{cases} \mathbf{F}_1^{\mathrm{s}} & \text{if } i = 1 \\ \mathbf{F}_i^{\mathrm{s}} - \mathbf{F}_{i-1}^{\mathrm{s}} & \text{if } 1 < i < N \\ -\mathbf{F}_{N-1}^{\mathrm{s}} & \text{if } i = N \end{cases} \quad (13)$$

where subscripts on the right-hand side of eq 13 refer to spring indices. We use the Marko–Siggia[38] expression for the restoring force of an entropic "wormlike" spring between two beads in the bead–spring chain:

$$\mathbf{F}_i^{\mathrm{s}} = \frac{kT}{b_{\mathrm{k}}} \left[\frac{1}{2} \frac{1}{\left(1 - \frac{Q}{Q_0}\right)^2} - \frac{1}{2} + \frac{2Q}{Q_0} \right] \frac{\mathbf{Q}_i}{Q} \quad (14)$$

where Q_0 is the maximum extensibility of a spring such that $Q_0 = N_{\mathrm{k,s}} b_{\mathrm{k}}$ and Q is the scalar magnitude of the spring extension vector $\mathbf{Q}_i$ for spring i. Equation 14 gives the wormlike chain (WLC) restoring force appropriate for double-stranded DNA.

Excluded-volume (EV) interactions are incorporated into our bead–spring model for polymer chains to accurately capture good solvent behavior of DNA in aqueous solution. EV interactions in polymer molecules have been studied extensively[39] and have well-known effects on the linear and nonlinear rheological properties of polymer solutions.[18,40–43] Intramolecular EV interactions occur when segments of a polymer molecule, which may be far separated along the chain, come into close approach; in this sense, they represent long-range interactions (long range with reference to distance along the polymer chain) with the overall effect of causing chain swelling at equilibrium. Physically, the molecular scale nature of EV interactions stems from steric repulsion between segments of a polymer chain. However, in real polymer chains, this "long-range" interaction is quite complicated and may include other effects such as van der Waals attraction and solvent-specific interactions, which may be lumped into EV interactions. Here, EV effects are modeled as short-range interactions that directly affect chain dynamics when two polymer segments (beads) come into close approach. The energy of interaction between beads i and j in a bead–spring chain can be expressed as[39]

$$U_{ij}^{\mathrm{EV}} = kT\bar{\nu}(\mathbf{r}_i - \mathbf{r}_j) \approx \nu kT\delta(\mathbf{r}_i - \mathbf{r}_j) \quad (15)$$

where $\bar{\nu}$ is a short-range excluded-volume function that attempts to account for EV interactions within a polymer chain. The vector between beads i and j is defined as $\mathbf{r}_{ij} = \mathbf{r}_j - \mathbf{r}_i$. The second expression in eq 15 is an approximation which models EV effects as extremely close-ranged interactions with the Dirac delta function, scaled in magnitude with the excluded-volume parameter ν. Although analytic calculations can incorporate the sharp Dirac delta function, a more convenient representation of $\delta(\mathbf{r}_i - \mathbf{r}_j)$ in Brownian dynamics simulation is a well-behaved generalized function in the form of a narrow Gaussian potential. Specifically, we employ an expression for the potential proposed in previous work[27] because it contains an explicit dependence on chain discretization:

$$U_{ij}^{\mathrm{EV}} = \frac{1}{2}\nu kT N_{\mathrm{k,s}}^2 \left(\frac{3}{4\pi R_{\mathrm{g,sub}}^2}\right)^{3/2} \exp\left[-\frac{3r_{ij}^2}{4R_{\mathrm{g,sub}}^2}\right] \quad (16)$$

where $|\mathbf{r}_{ij}| = r_{ij}$ and $R_{\mathrm{g,sub}} = \sqrt{(N_{\mathrm{k,s}} b_{\mathrm{k}}^2)/6}$ is the radius of gyration of a subsection of the polymer chain. After taking the gradient of the potential and scaling by appropriate quantities, we arrive at an expression for the dimensionless EV force on bead i:

$$\mathbf{F}_i^{\mathrm{EV}} = -\sum_{j=1; i \neq j}^{N} \sqrt{3}z \left(\frac{9}{2}\right) \exp\left[-\frac{3r_{ij}^2}{2}\right]\mathbf{r}_{ij} \quad (17)$$

where $z = (1/2\pi)^{3/2} \tilde{\nu} N_{\mathrm{k,s}}^2$ and the dimensionless EV parameter is $\tilde{\nu}$. The expression for the energy of interaction between two beads due to excluded volume given in eq 16 is convenient to use for BD simulations of bead–spring polymer chains because it directly depends on chain discretization through the quantity $R_{\mathrm{g,sub}}$, the radius of gyration of a chain subunit. It is well-known from perturbation analysis[39,42] that corrections to the end-to-end vector for free-draining polymer chains due to EV interactions scale as $(\nu/b_{\mathrm{k}}^3)\sqrt{N}$ or $\tilde{\nu}\sqrt{N}$ (neglecting a numerical constant). It has been demonstrated[27] that eq 16 yields the correct parameter dependence in the scaling of equilibrium polymer properties such as radius of gyration and center-of-mass diffusivity. In short, for a given value of the dimensional EV parameter ν, good solvent polymer behavior is recovered when the polymer contour length L is fixed and the chain discretization $N_{\mathrm{k,s}}$ (and hence number of springs N_{s}) is varied. The factor of $N_{\mathrm{k,s}}^2$ explicitly appears in eq 16 so that the quantity ν may be set at a fixed value when varying the level of chain discretization while maintaining the static, equilibrium polymer properties at a constant value. Equivalently, for a fixed value of ν, one may fix $N_{\mathrm{k,s}}$ and simulate longer chains by increasing N_{s} while recovering the good solvent scaling properties as a function of molecular weight.

Prakash and co-workers have recently published several detailed articles investigating the influence of excluded-volume interactions on Hookean dumbbells and Rouse chains both at equilibrium and in flow.[40–42] Expressed in the notation of Prakash,[42] eq 16 may be rewritten:

$$U_{ij}^{\mathrm{EV}} = \frac{1}{2}\frac{z^*}{(d^*)^3}kT N_{\mathrm{k,s}}^2 \exp\left(-\frac{1}{2}\frac{H}{kT}\frac{r_{ij}^2}{(d^*)^2}\right) \quad (18)$$

where $z^* = \nu(H/2\pi kT)^{3/2} = \tilde{\nu}(1/2\pi)^{3/2}$. Note that z is related to z^* such that $z = z^* N_{\mathrm{k,s}}^2$. The quantity d^* in eq 18 is related to the width of the narrow Gaussian potential, and $(d^*)^2$ was set to $1/3$ to relate eqs 16 and 18.

3.2. Algorithm. We employ a highly efficient predictor–corrector algorithm to solve the set of eqs 12 for the spring connector vectors at each time step. This algorithm was originally proposed for general free-draining bead–spring chains.[37] Recently, it was extended to model polymers with fluctuating HI[17] and shown to be significantly more efficient than either explicit Euler or iterative Newton solution schemes. In this work, we modify the original model as described by Somasi et al.[37] to include both fluctuating intrachain HI *and* excluded-volume interactions.

The first step in the algorithm involves a simple Euler predictor step for spring i:

$$\mathbf{Q}_i^* = \mathbf{Q}_i^n + [Pe(\kappa\cdot\mathbf{Q}_i^n) + \sum_{j=1}^N (\mathbf{D}_{i+1,j}^n - \mathbf{D}_{i,j}^n)\cdot(\mathbf{F}_j^{E,n} +$$

$$\mathbf{F}_j^{EV,n})]\,\mathrm{d}t + \sqrt{2}\sum_{j=1}^i (\alpha_{i+1,j}^n - \alpha_{i,j}^n)\cdot\mathrm{d}\mathbf{W}_j \quad (19)$$

where $\mathbf{Q}_i^*$ is the intermediate Euler predicted connector vector for spring i. The quantity $\mathbf{Q}_i^*$ from the Euler predictor step is subsequently used in the first corrector step:

$$\bar{\mathbf{Q}}_i + (\mathbf{D}_{i+1,i+1}^n + \mathbf{D}_{i,i}^n)\cdot\bar{\mathbf{F}}_i^s\,\mathrm{d}t =$$

$$\mathbf{Q}_i^n + \left[\frac{1}{2}Pe(\kappa\cdot\mathbf{Q}_i^n + \kappa\cdot\mathbf{Q}_i^*) + (\mathbf{D}_{i+1,i+1}^n + \mathbf{D}_{i,i}^n)\cdot\mathbf{F}_i^{s,n} +\right.$$

$$\left.\sum_{j=1}^N (\mathbf{D}_{i+1,j}^n - \mathbf{D}_{i,j}^n)\cdot(\mathbf{F}_j^E + \mathbf{F}_j^{EV,n})\right]\mathrm{d}t +$$

$$\sqrt{2}\sum_{j=1}^i (\alpha_{i+1,j}^n - \alpha_{i,j}^n)\cdot\mathrm{d}\mathbf{W}_j \quad (20)$$

where $\mathbf{F}_j^E = \bar{\mathbf{F}}_j^E$ if $j < i$; else $\mathbf{F}_j^E = \mathbf{F}_j^{E,n}$. The right-hand side of eq 20 is completely determined for spring i, and solution for $\bar{\mathbf{Q}}_i$ on the left-hand side of eq 20 is achieved with a cubic solver. We have moved the diagonal terms involving $\mathbf{D}$ to the left-hand side of eq 20 and added a similar term to the right-hand side, which allows us to keep the summation intact as suggested by Hsieh et al.[17] Finally, an iterative step is implemented using the corrected value for the connector vector for spring i from the second step:

$$\mathbf{Q}_i^{n+1} + (\mathbf{D}_{i+1,i+1}^n + \mathbf{D}_{i,i}^n)\cdot\mathbf{F}_i^{s,n+1}\,\mathrm{d}t =$$

$$\mathbf{Q}_i^n + \left[\frac{1}{2}Pe(\kappa\cdot\mathbf{Q}_i^n + \kappa\cdot\bar{\mathbf{Q}}_i) + (\mathbf{D}_{i+1,i+1}^n + \mathbf{D}_{i,i}^n)\cdot\bar{\mathbf{F}}_i^{s,n} +\right.$$

$$\left.\sum_{j=1}^N (\mathbf{D}_{i+1,j}^n - \mathbf{D}_{i,j}^n)\cdot(\mathbf{F}_j^E + \mathbf{F}_j^{EV,n})\right]\mathrm{d}t +$$

$$\sqrt{2}\sum_{j=1}^i (\alpha_{i+1,j}^n - \alpha_{i,j}^n)\cdot\mathrm{d}\mathbf{W}_j \quad (21)$$

where $\mathbf{F}_j^E = \mathbf{F}_j^{E,n+1}$ if $j < i$; else $\mathbf{F}_j^E = \bar{\mathbf{F}}_j^{E,n}$. The iteration tolerance is satisfied when $\epsilon = [\sum_{i=1}^{Ns}(\mathbf{Q}_i^{n+1} - \bar{\mathbf{Q}}_i)^2]^{1/2}$ is less than a small number (typically 10^{-6} for this work). The mobility tensor $\mathbf{D}_{ij}$ and the excluded-volume forces $\mathbf{F}_i^{EV}$ are updated at the beginning of each time step. Cholesky's method[44] is used to decompose the mobility tensor and to calculate the coefficient tensor α_{ij} at the start of each time step. Cholesky's method may be used to factor a symmetric, positive definite tensor (these qualities are conveniently guaranteed by choosing $\mathbf{D}_{ij}$ as the RPY tensor) through a modified lower−upper matrix factorization; however, it is notably expensive to perform with the total number of calculations scaling as N^3 for a square $3N \times 3N$ matrix. Spectral methods employing Chebyshev polynomials have recently been used to approximate the vector $\alpha_{ij}\cdot\mathbf{W}_j$[45,27] (rather than calculation of the coefficient tensor α_{ij}) using a method originally proposed by Fixman.[46] The advantage of Fixman's method lies in computational savings, as the spectral approximation scales as $N^{2.25}$ for polymer chains with excluded-volume interactions. As noted by Jendrejack et al.,[45] Fixman's method is facilitated by inclusion of EV interactions. In the absence of EV interactions, beads may significantly overlap; as bead overlap increases, the number of terms required to be retained in the spectral approximation (for a given accuracy) increases. In the limit of large bead overlap, as often encountered in coiled polymer configurations, Cholesky's method becomes faster than the spectral approximation.

3.3. Choice of Model Parameters. Our bead−spring model contains five parameters that are chosen in a systematic manner for DNA molecules. First, the Kuhn step size (b_k) is well-known for dsDNA stained with YOYO-1 dye and generally should not be treated as an adjustable parameter. At the dye concentrations similar to those used in our experiments, b_k was found to increase by a factor of 1.32 from the native value of approximately 100 nm for unstained DNA in aqueous solution containing at least 10 mM monovalent salt.[11] Therefore, we take b_k to be 0.132 μm. Next, we choose the quantity $N_{k,s}$ for a given level of discretization, and the number of springs $N_s = (N − 1)$ is set by the constraint that the dimensional contour length $L = N_{k,s}N_sb_k$ is maintained at a chosen value. For simulations of 7-lambda (150 μm) DNA, we use 28 springs and set $N_{k,s} = 40$. For simulations of 340 μm DNA, we keep the same level of discretization ($N_{k,s} = 40$) and increase N_s to 64. Only two parameters in the model remain: the bead radius (a) appearing in the RPY tensor and the excluded-volume parameter (ν).

We applied two different methods for choosing the bead radius a and the EV parameter ν for DNA chains. The first scheme involved choosing a and ν such that the BD simulations reproduce both the experimental center-of-mass diffusivities (D)[11] and relaxation times (τ) for DNA of contour length L. This parameter scheme was possible for 150 and 340 μm DNA, but not for 1300 μm DNA due to lack of equilibrium center-of-mass diffusivity data for this length molecule. The second method was applied to 1300 μm long DNA. In this case, we choose a and ν such that the simulations reproduce the experimental relaxation time and the average polymer stretch at flow strengths below the coil−stretch transition (see section 4). As discussed below, the paramters a and ν for 1300 μm DNA were also used to simulate the behavior of 150 and 340 μm DNA. Longest polymer relaxation times are calculated in the same manner in experiment as in simulation as described in section 2.3. The radius of gyration (R_g) of DNA stained with dye cited in previous work[11] is calculated using the results of Zimm theory and the experimentally measured diffusivities, and we therefore choose not to match R_g from simulation to these calculated quantities.

Center-of-mass chain trajectories were tracked to extract chain diffusivities (D). The center-of-mass position of a polymer may be calculated by

$$\mathbf{r}_c^{n+1} = \mathbf{r}_c^n + \frac{1}{N}\sum_{i=1}^N \mathrm{d}\mathbf{r}_i \quad (22)$$

The ensemble averaged distance that the polymer center of mass travels at time t is given by

$$\langle \mathbf{r}_c^2 \rangle = \frac{1}{M} \sum_{i=1}^{M} (\mathbf{r}_{c,i}^t - \mathbf{r}_{c,i}^0)^2 \tag{23}$$

where $\mathbf{r}_{c,i}^0$ is the initial center-of-mass position for chain i in an ensemble containing M polymer molecules. A plot of $\langle \mathbf{r}_c^2 \rangle$ vs dimensionless time gives the coefficient $6\tilde{D}$, where $\tilde{D}$ is the ensemble-averaged dimensionless diffusivity. In general, molecular ensemble sizes for relaxation time and diffusivity simulations involved ≈ 60 and $\approx 300-500$ molecules, respectively.

Using the first method described above, we arrived at the following set of parameters for BD simulations of 7-lambda DNA: $N_{k,s} = 40$, $N_s = 28$, $b_k = 0.132$ μm, $a = 0.101$ μm (or $h^* = 0.12$), and $\nu = 0.0034$ μm^3. This parameter set yielded an average diffusivity of $D = 0.169$ μm^2/s in a 0.95 cP solvent and relaxation time τ of 21.0 s in an 8.4 cP buffer, values that are 5% and 3.5% larger than experimentally measured quantities. To test the robustness of our parameter matching scheme, we relaxed the requirement of a fixed Kuhn step size. For 7-lambda DNA, choosing $N_{k,s} = 42.9$, $N_s = 28$, $b_k = 0.118$ μm, $a = 0.12$ μm (or $h^* = 0.15$), and $\nu = 0.0049$ μm^3 gave $D = 0.166$ μm^2/s and $\tau = 20.2$ s. Although this parameter set gives smaller errors in D and τ than the above set for $b_k = 0.132$ μm, as discussed in section 4, the transient molecular stretch results are more accurate for the parameter set keeping b_k fixed at its known experimental value. For DNA with $L = 340$ μm, we kept a (or h^*) and ν at the same values as for 7-lambda DNA; with the same discretization level ($N_{k,s} = 40$), we increased the number of springs N_s to 64 and found $D = 0.099$ μm^2/s in 0.95 cP solvent and $\tau = 11.1$ s in 1.0 cP solvent. These quantities are in excellent agreement with experimental values for DNA stained with YOYO-1 dye. Accurate scaling of D and τ upon increasing only the total length of the chain (number of springs) is comforting.

For 1300 μm long DNA, we choose our simulation parameters using the second method described above. First, the number of Kuhn steps per spring is increased by a factor of 2 to allow for simulation of large DNA chains in reasonable time frames. Furthermore, the Kuhn step size is maintained at a constant value, giving $N_{k,s} = 80$, $N_s = 123$, and $b_k = 0.132$ μm. (We assume that b_k remains constant at 0.132 μm even though the experiments involving 1300 μm DNA were done using Sytox Green dye, and it is possible that Sytox may affect the Kuhn step size slightly differently than YOYO-1.) Here, we choose a and ν to match the experimental relaxation time and experimental polymer stretch at low De (=0.30), giving $a = 0.28$ μm (or $h^* = 0.23$) and $\nu = 0.000\,32$ μm^3. These parameters give $\tau = 126$ s and fractional polymer stretch $\langle x \rangle / L$ of 0.014 as determined in previous work.[29]

Finally, we also simulated the transient flow behavior of 150 and 340 μm DNA using the parameters a and ν originally chosen for 1300 μm DNA. For 150 μm DNA, the parameter set becomes $N_{k,s} = 40$, $N_s = 28$, $b_k = 0.132$ μm, $a = 0.20$ μm (or $h^* = 0.23$), and $\nu = 0.000\,32$ μm^3. This set of parameters yielded $D = 0.163$ μm^2/s in 0.95 cP solvent and $\tau = 29.7$ s in 8.4 cP solvent. In this case, the error in the relaxation time is large. Reducing the Kuhn step size *slightly* to $b_k = 0.12$ μm gives $D = 0.179$ μm^2/s and $\tau = 22.3$ s, values which are only 15% and 9% larger than experimentally measured quantities. We also applied these parameter choices to 340 μm DNA, giving $N_{k,s} = 40$, $N_s = 64$, $b_k = 0.132$ μm, $a = 0.20$ μm

(or $h^* = 0.23$), and $\nu = 0.000\,32$ μm^3. This set of parameters yielded $D = 0.113$ μm^2/s in 0.95 cP solvent and $\tau = 12.7$ s in 1 cP solvent, values which are 16% and 13% larger than experimentally measured quantities.

3.4. Conformation-Dependent Resistivity. Hydrodynamic interactions in polymer molecules give rise to conformation-dependent resistivities. It is predicted that the hydrodynamic drag on a polymer chain can increase significantly as the molecule extends from the coiled to extended state; in the fully extended configuration, polymer segments are separated, and the effects of intrachain HI diminish. In the extended conformation, the fluid is able to exert a stronger frictional grip on the polymer. This phenomenon was observed to give rise to polymer conformation hysteresis in planar extensional flow in recent work.[29] We can estimate the polymer drag coefficient in the coiled state (ζ^{coil}) from Zimm theory (assuming a good solvent), and we employ Batchelor's slender body theory[47] to approximate the drag in the fully extended state ($\zeta^{stretch}$) equal to the drag on a rigid rod in viscous flow. Ignoring a log term, the ratio $\zeta^{stretch}/\zeta^{coil}$ scales with polymer molecular weight M as $M^{0.4}$ in uniform flow and as $M^{1.4}$ in planar extensional flow. Therefore, the effects of conformation-dependent drag on the dynamics of polymers are expected to become more important for larger or highly extensible polymers.

In this section, we describe calculation of polymer resistivity $\zeta(R)$ as a function of polymer stretch R. In the simulation, we calculate the external force required to fix the polymer molecule at various extensions (R) with and without flow. Essentially, this procedure amounts to calculation of the *conformation-dependent hydrodynamic force exerted on the polymer by the solvent* in a planar extensional flow. We calculate the resistivity $\zeta(R)$ of a multi-bead–spring chain to use the information in coarse-grained dumbbell models to calculate effective conformational energies in extensional flows and ensemble averaged stretch using kinetic theory, as described in section 3.6.

We begin by fixing the end beads of a multi-bead–spring polymer in a planar extensional flow such that end beads are a distance $\pm R/2$ from the origin along the principal axis of extension. In the dimensionless connector vector equations for springs 1 and N_s, the quantities $d\mathbf{r}_1$ and $d\mathbf{r}_{N_s+1}$ are set to zero. The external force required to maintain the end bead N fixed in space is $\mathbf{F}^{Ext}$ and may be expressed as

$$\mathbf{F}^{Ext} = -\mathbf{F}^{Hyd} - \mathbf{F}^E - \mathbf{F}^{Br} \tag{24}$$

where $\mathbf{F}^{Hyd}$ is the hydrodynamic force exerted by the fluid on the bead, $\mathbf{F}^E$ is the entropic spring force, and $\mathbf{F}^{Br}$ is the random Brownian force on the end bead. Clearly, $\mathbf{F}^{Hyd}$ depends on the configuration of the macromolecule at each time step. In dimensionless form, the hydrodynamic force on bead $i = N$ is

$$\mathbf{F}_i^{Hyd} = \sum_{j=1}^{N} \zeta_{ij} \cdot \left[Pe(\kappa \cdot \mathbf{r}_j) - \frac{d\mathbf{r}_j}{dt} \right] \tag{25}$$

where $\zeta_{ij} = \mathbf{D}_{ij}^{-1}$. The quantity we actually seek is $\langle \mathbf{F}^{Hyd} \rangle$, so we ensemble average eq 24 and take advantage of the isotropic nature of random Brownian forces such that $\langle \mathbf{F}^{Br} \rangle = 0$. Furthermore, we can express the hydrodyamic force in terms of the spring forces to avoid

calculations based on noisy instantaneous bead velocities and arrive at

$$\langle \mathbf{F}_i^{\text{Hyd}} \rangle = \sum_{j=1}^{N} \begin{cases} \langle \zeta_{ij} \cdot Pe(\kappa \cdot \mathbf{r}_j) \rangle & \text{if } j = 1 \text{ or } N \\ -\sum_{k=1}^{N} \langle \zeta_{ij} \cdot \mathbf{D}_{jk} \cdot \mathbf{F}_k^E \rangle & \text{if } j = 2, N-1 \end{cases} \quad (26)$$

For beads $j = 1$ or N, $(\mathrm{d}\mathbf{r}_j/\mathrm{d}t) = 0$, which simplifies calculations as shown in the second expression in eq 26. The entropic spring force exerted on the end bead may be readily calculated.

We can now calculate the external force required to hold either end bead fixed as a function of chain extension under both equilibrium and flow conditions. The drag on one end bead in a coarse-grained variable resistivity dumbbell can then be calculated from

$$\zeta(R) = \frac{\langle F^{\text{Ext}}(R) \rangle \mid_{\text{eq}} - \langle F^{\text{Ext}}(R) \rangle \mid_{\text{flow}}}{2PeR} \quad (27)$$

ζ is a function of chain stretch and an implicit function of flow strength De, so we perform these calculations at different De values.

3.5. Brownian Dumbbells: Variable Resistivity. In addition to a multi-bead−spring polymer chain with fluctuating HI, we have constructed a coarse-grained Brownian dumbbell algorithm with conformation-dependent resistivity. Previous work[48] has demonstrated that care must be taken in constructing Brownian algorithms with variable diffusivities: erroneous results will be obtained when naive forward time stepping of the stochastic differential equation describing the bead connector vector is carried out with the constant resistivity ζ replaced with variable resistivity $\zeta(Q)$. In the case of point particle diffusion, regions of low resistivity (high diffusivity) become depleted of particles due to more vigorous Brownian forces in these regions. There are several methods to correct for this complication. Ermak and McCammon[33] explicitly add a drift velocity term to the stochastic differential equation in a simple Euler time stepping algorithm; however, this method requires calculation of the spatial derivatives of the diffusivity tensor $\mathbf{D}_{ij}$. Fixman[49] suggested an alternative midpoint method where the random Brownian force is kept at a constant value over the time step. One can show that these two formulations are equivalent upon expanding the resistivity in small powers of $\mathrm{d}t$ in the final step of the midpoint algorithm. We propose a third algorithm in which the resistivity in the random Brownian term varies throughout the time step. This algorithm is novel because we solve for the dumbbell connector vector via a semiimplicit solver similar to that proposed by Somasi et al.[37] for multi-bead−spring chains. The first Euler predictor step for the spring extension in dimensionless form is

$$\mathbf{Q}^* = \mathbf{Q}^n + \mathrm{d}t \left[Pe(\kappa \cdot \mathbf{Q}^n) - \frac{2}{\zeta(Q^n)} \mathbf{F}^{E,n} \right] + \\ \sqrt{\frac{\mathrm{d}t}{2\zeta(Q^n)}} (\mathbf{n}_1 - \mathbf{n}_2) \quad (28)$$

where $\zeta(Q)$ is the dimensionless conformation-dependent resistivity per bead scaled with the Zimm value and $\mathbf{n}_i$ is a random Gaussian vector distributed vector over $[-1, 1]$ with zero mean and variance of 1 for beads $i =$

1 or 2. The value for the predicted extension is used in the corrector step of the algorithm:

$$\mathbf{Q}^{n+1} = \mathbf{Q}^n + \frac{\mathrm{d}t}{2} \Bigg[Pe(\kappa \cdot \mathbf{Q}^n + \kappa \cdot \mathbf{Q}^*) - \\ 2\left(\frac{1}{\zeta(Q^n)} \mathbf{F}^{E,n} + \frac{1}{\zeta(Q^*)} \mathbf{F}^{E,n+1} \right) \Bigg] + \\ (\mathbf{n}_1 - \mathbf{n}_2) \left(\sqrt{\frac{\mathrm{d}t}{2\zeta(Q^n)}} + \sqrt{\frac{\mathrm{d}t}{2\zeta(Q^*)}} \right) \quad (29)$$

Solution for the spring extension Q^{n+1} in eq 29 can be obtained via a cubic routine. It is apparent from eq 29 that the frictional terms in the random Brownian forces do indeed vary over the time step $\mathrm{d}t$. It should be noted that this algorithm constitutes a two-step procedure similar to the algorithm suggested by Öttinger,[15] and unlike the multi-bead−spring algorithm presented in section 3.2, no iterative step follows the corrector step in eq 29.

3.6. Kinetic Theory: Variable Drag WLC Dumbbells. In this section, we describe calculation of transient and steady ensemble average end-to-end extension of a dumbbell with variable drag in planar extensional flow using kinetic theory. We employ the $\zeta(R)$ functionality from the multi-bead−spring chain as described in section 3.4 and use a WLC force law for the entropic spring between two beads experiencing conformation-dependent drag. We begin by considering the configuration-space distribution function Ψ for polymer extension, invoking the usual assumption that the phase-space distribution function F may be written as a product of the configuration-space function Ψ and a velocity-space distribution function Ξ, such that $F = \Psi\Xi$.[34] We assume that the velocity distribution is Maxwellian about the solvent velocity and hence consider only the configuration-space function Ψ. The configuration-space distribution function may be expressed in center-of-mass position and dumbbell extension coordinates such that

$$\Psi = \Psi(\mathbf{x}, \mathbf{R}, t) = n\psi(\mathbf{R}, t) \quad (30)$$

where $\mathbf{x}$ is the vector giving the center-of-mass position of a dumbbell and $\mathbf{R}$ is the end-to-end vector of the dumbbell. The second expression in eq 30 results from the assumption that the dumbbell configuration is independent of the center-of-mass position, and n is the number concentration of dumbbells. We normalize ψ with the condition: $\int \psi \, \mathrm{d}\mathbf{R} = 1$. The equation of motion for the dumbbell end-to-end vector may be written as

$$\frac{\mathrm{d}R_i}{\mathrm{d}t} = \kappa_{ij} R_j - \frac{2Hf(|R|)R_i}{\zeta(R)} - \frac{2kT}{\zeta(R)} \frac{\partial}{\partial R_i} \log \psi \quad (31)$$

where subscripts in this subsection and the next refer to tensorial indices. The WLC chain force law has been expressed as $F_i = Hf(|R_i|/L)R_i$ such that the quantity f describes the nonlinear response of the spring and accounts for finite extensibility. For polymers obeying a wormlike chain force law

$$f\left(\frac{|R_i|}{L} \right) = \frac{L}{6R} \left[\frac{4R}{L} + \frac{1}{(1 - R/L)^2} - 1 \right] \quad (32)$$

where $R = |R_i|$. Furthermore, we assume that κ_{ij} is a constant function of position such that

$$\kappa_{ij} = \begin{pmatrix} \dot{\epsilon} & 0 & 0 \\ 0 & -\dot{\epsilon} & 0 \\ 0 & 0 & 0 \end{pmatrix} \quad (33)$$

We employ eq 31 in the Fokker–Planck equation describing the configuration-space distribution function ψ:

$$\frac{\partial \psi}{\partial t} = -\frac{\partial}{\partial R_i}\left(\frac{\partial R_i}{\partial t}\psi\right) \quad (34)$$

We multiply eq 34 by $R_i R_j$ and integrate over configuration space, using Gauss' theorem and assuming that ψ decays to zero as $|r_i| \rightarrow \infty$. Finally, we nondimensionalize length with the quantity $\sqrt{kT/H}$ and time with the appropriate convective time scale $\dot{\epsilon}$, giving

$$\frac{dA_{ij}}{dt} = \kappa_{ik}A_{kj} + \kappa_{jk}A_{ki} - \frac{\zeta_0}{De\zeta(R)}(fA_{ij} - \delta_{ij}) \quad (35)$$

where the second moment of R_i is defined by $A_{ij} = \langle R_i R_j \rangle$, and the Deborah number $De = \dot{\epsilon}\tau_{Zimm}$ is based on the Zimm relaxation time. The quantity $\zeta(R)/\zeta_0$ is the conformation-dependent resistivity *per bead* from section 3.4 normalized by the equilibrium Zimm value (ζ_0). We assume that the nonlinear spring force and the resistivity are both functions of the instantaneous ensemble averaged end-to-end spring extension such that $f(R) = f(A_{ii}^{1/2})$ and $\zeta(R) = \zeta(A_{ii}^{1/2})$. Similar derivations for polymer dumbbells using a preaveraged Warner force law and a preaveraged linearly increasing drag coefficient have been presented.[30,50] Equations 35 represent a nonlinear, nonhomogeneous set of ordinary differential equations for A_{ij}, which can be solved for A_{11}, A_{22}, and A_{33} as functions of time using a fourth-order Runge–Kutta scheme.

3.7. Effective Conformational Energy. In addition to employing kinetic theory to calculate transient ensemble average molecular extension as described in section 3.6, we describe a method to calculate the effective conformational energy of a polymer in flow as originally suggested by de Gennes in this context.[51] We again use the dumbbell model for a polymer with variable bead resistivity and define a dimensionless conformation-dependent drag coefficient $g(R)$:

$$g(R) = \frac{\zeta(R)}{\zeta_0} \quad (36)$$

such that the resistivity coefficient per bead is normalized by the Zimm value ζ_0. Beginning with the Fokker–Planck equation, we seek steady solutions for ψ such that $\partial\psi/\partial t = 0$. Equation 34 reduces to

$$\frac{\partial}{\partial R_i}(\kappa_{ij}R_j\psi) - \frac{\partial}{\partial R_i}\left(\frac{2H}{\zeta_0}\frac{f(R)}{g(R)}R_i\psi\right) = \frac{\partial}{\partial R_i}\left(\frac{2kT}{\zeta_0 g(R)}\delta_{ij}\frac{\partial \psi}{\partial R_j}\right) \quad (37)$$

Equation 37 results from setting the divergence of the probability flux is equal to zero. For steady, spatially homogeneous, incompressible potential flows, it is well-known that an analytical solution for ψ exists when the resistivity coefficient ζ is constant.[34,52] However, we seek solutions for ψ such that the resistivity ζ is a function of polymer extension, and such an analytical solution is not immediately obvious. We begin by nondimension-

alizing eq 37 with length scale $l_s = \sqrt{kT/H}$ and time with the relaxation time of a Hookean dumbbell $\tau_r = \zeta_0/4H$. Defining a dimensionless length $\xi = R/l_s$, we arrive at

$$2De\frac{\partial}{\partial \xi_i}(\tilde{E}_{ij}\xi_j\psi) - \frac{\partial}{\partial \xi_i}\left(\frac{f(\xi)}{g(\xi)}\xi_i\psi\right) = \frac{1}{2}\frac{\partial}{\partial \xi_i}\left(\frac{\delta_{ij}}{g(\xi)}\frac{\partial \psi}{\partial \xi_j}\right) \quad (38)$$

where the velocity gradient tensor is $\kappa_{ij} = \dot{\epsilon}\tilde{E}_{ij}$ and $\tilde{E}_{ij} = \delta_{i1}\delta_{j1} - \delta_{i2}\delta_{j2}$. We make analytical progress by assuming that for planar extensional flow, polymer extension in the direction of the principal axis of stretch is much greater than in the principal axis of compression direction, such that $\xi_1 \gg \xi_2$, giving $g(\xi) \approx g(\xi_1)$ and $f(\xi) \approx f(\xi_1)$. Defining the quantity $\phi = \phi(\xi_1)$

$$\phi(\xi_1) = \int_{-\infty}^{+\infty}\psi(\xi_1, \xi_2, \xi_3)\,d\xi_2\,d\xi_3 \quad (39)$$

we can express eq 38 as a function of ξ_1. We are now able to write an expression for ϕ directly:

$$\phi(\xi_1; De) = K\exp\{-\int_0^{\epsilon_1}(\sigma f(\sigma) - 2De\sigma g(\sigma))\,d\sigma\} \quad (40)$$

with the constant K defined from the normalization condition $\int_{-\infty}^{+\infty}\phi\,d\xi_1 = 1$. Finally, we can define a dimensionless effective conformational energy:

$$\frac{E(\xi_1; De)}{kT} = \int_0^{\epsilon_1}(\sigma f(\sigma) - 2De\sigma g(\sigma))\,d\sigma \quad (41)$$

The analysis presented in this section was motivated by the work of de Gennes,[51] who sketched the results of such an analysis with neither formal proof nor quantitative values for $\zeta(R)$ and $f(R)$. Of course, we are merely drawing an analogy (through the approximate Boltzmann distribution) between the present nonequilibrium problem and traditional equilibrium statistical mechanics,[53] as the stationary distribution in this case does not imply thermal equilibrium.[51] Nevertheless, calculation of effective polymer conformational energies via eq 41, or equivalently the probability distribution of extension, is useful for polymer chains that exhibit hysteresis.[29]

4. Results and Discussion

We begin by comparing transient molecular extension obtained from both single molecule visualization experiments and Brownian dynamics simulations including HI and EV interactions. Figure 1a–c shows the transient fractional molecular extension for 7-lambda DNA molecules ($L \approx 150\ \mu m$) in a planar extensional flow for $De = $ (a) 0.75, (b) 0.98, and (c) 4.0. Individual molecular trajectories from the experiments are shown in light gray traces, and the ensemble average data from the experiments and simulation are also shown. Good agreement between experiment and simulation at $De = 0.75$ and 0.98 is obtained using $N_s = 28$, $N_{k,s} = 40$, $h^* = 0.12$, and $\nu = 0.0034\ \mu m^3$ where the equilibrium chain diffusivity D and relaxation time τ are matched to experimentally measured values, as described in section 3.3. Not surprisingly, the ensemble averaged trajectories from the BD simulation begin to deviate slightly from experimental averages at a larger value of $De = 4.0$. Because model parameters are chosen to reproduce equilibrium (or near-equilibrium) polymer properties, some disagreement with simulation may be
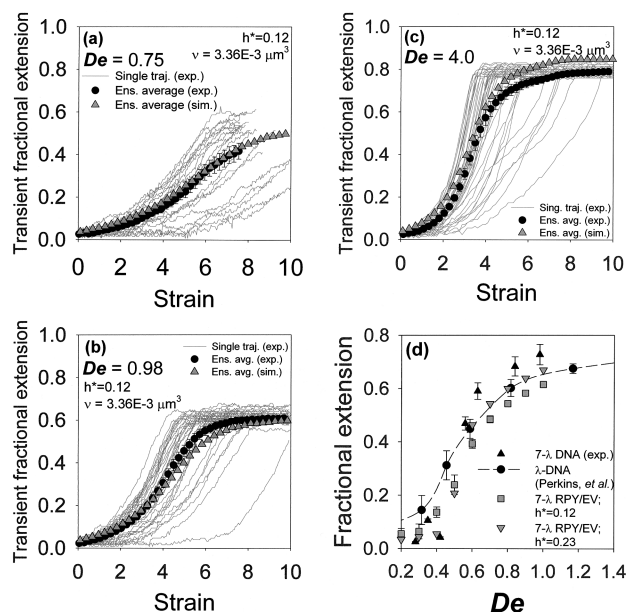
Figure 1. Transient fractional molecular extension for 7-lambda ($L = 150 \ \mu$m) DNA in planar extensional flow, single molecule experiment, and Brownian dynamics simulation, for (a) $De = 0.75$, (b) $De = 0.98$, and (c) $De = 4.0$. (d) Steady-state fractional polymer extension for 7-lambda DNA and lambda DNA[7] in planar extensional flow.

expected at highly nonequilibrium polymer configurations realized at large values of De.

Figure 1d shows steady-state polymer extension for 7-lambda DNA from BD simulations and single molecule experiments. Also plotted in Figure 1d is the steady-state fractional molecular extension for lambda DNA in planar extensional flow from previous work.[7] Experimental results clearly show that the coil−stretch transition steepens as the effects of HI become increasingly important for larger DNA chains. Although the parameter set chosen for 7-lambda DNA such that BD simulations reproduce experimental D and τ ($h^* = 0.12$ and $\nu = 0.0034 \ \mu$m^3) accurately captures transient molecular extension behavior for 7-lambda DNA as shown in Figure 1a−c (within acceptable error), the same parameter set does not accurately predict steady-state chain extension. Rather, the second parameter set ($h^* = 0.23$ and $\nu = 0.000 \ 32 \ \mu$m^3) originally chosen for 1300 μm DNA as described in section 3.3 shows a sharper coil−stretch transition and better predicts experimental data for 7-lambda DNA. For experimental studies of steady-state extension of 7-lambda DNA and for all 1300 μm DNA experiments, Sytox Green dye was used to stain the DNA. It is possible that Sytox affects the Kuhn step size slightly differently than YOYO-1 which could impact parameter choices, as the time scale used to dimensionalize relaxtion time from BD simulation is proportional to $b_k{}^3$. Of course, we expect the qualitative polymer response (e.g., the steepening of the coil−stretch transition upon increasing polymer molecular weight) to be independent of the choice of fluorescent dye.

Figure 2a−c shows the ensemble averaged transient molecular extension from experiments, the free-draining BD algorithm (with $h^* = 0$ and $\nu = 0$), and for the BD algorithm with fluctuating HI and EV interactions with both sets of parameter choices for a and ν. In Figure 2a,b, results for the free-draining polymer chains show a marked disagreement with both experiments and BD
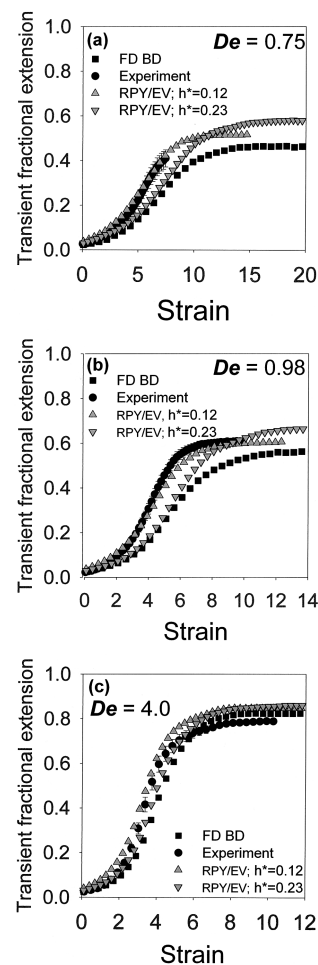

Figure 2. Ensemble averaged transient fractional molecular extension: experiment, BD simulation with HI and EV interactions and BD simulations of free-draining 7-lambda DNA chains for (a) $De = 0.75$, (b) $De = 0.98$, and (c) $De = 4.0$. Results from BD simulations with HI/EV for two different parameter sets are shown: $h^* = 0.12$ and $\nu = 3.36 \times 10^{-3} \ \mu$m^3 and also $h^* = 0.23$ and $\nu = 3.17 \times 10^{-4} \ \mu$m^3.

simulations with HI/EV using the first set of parameters ($h^* = 0.12$ and $\nu = 0.0034 \ \mu$m^3, such that D and τ are matched to experimental values). Better agreement between the FD simulation and experiments at $De = 4.0$ is shown in Figure 2c as molecules exhibit larger degrees of stretch, and the effects of HI diminish. Interestingly, FD simulation results closely follow BD results for chains with HI/EV for the second parameter set ($h^* = 0.23$ and $\nu = 0.000 \ 32 \ \mu$m^3) up to accumulated fluid strains of ≈ 5 for $De = 0.75$ and 0.98, before deviating to larger values of fractional molecular stretch. As the role of intramolecular HI becomes increasingly more important as h^* changes from 0.12 to 0.23, the transient molecular stretch at low values of accumulated fluid strain is smaller, which suggests that HI tends to slow down the onset of molecular stretch. However, BD simulations with larger values of h^* lead to larger steady-state plateau values of molecular extension. As shown in Figure 1d, as h^* increases, the coil−stretch transition for 7-lambda DNA steepens. Finally, it should be noted that these results demonstrate that incorporation of intramolecular hydrodynamic interactions is necessary for an accurate dynamical description of DNA molecules only 7 times as long as lambda DNA.
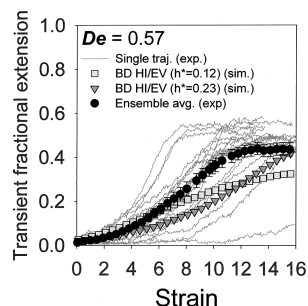
Figure 3. Transient fractional molecular extension for 340 μm DNA in planar extensional flow, single molecule experiment, and Brownian dynamics simulation, for $De = 0.57$. Results from BD simulations with HI/EV for two different parameter sets are shown: $h^* = 0.12$ and $\nu = 3.36 \times 10^{-3}$ μm^3 and also $h^* = 0.23$ and $\nu = 3.17 \times 10^{-4}$ μm^3.

Next, we investigated the dynamics of larger DNA chains in planar extensional flow. Figure 3 shows the transient fractional molecular extension for DNA with $L \approx 340$ μm. As discussed in section 3.3, two different sets of parameters (h^* and ν) were used in simulations of 150 and 340 μm DNA. For the first set of parameters for 340 μm DNA, we fixed the HI and EV parameters at the same values as for 7-lambda DNA ($h^* = 0.12$ and $\nu = 0.0034$ μm^3), maintained the same level of discretization ($N_{k,s} = 40$), and simply increased the number of springs to $N_s = 64$. Although the correct equilibrium diffusivity and relaxation time were extracted from the simulation with the parameter set, there is some disparity between the ensemble average transient polymer extension from simulation and experiment as shown in Figure 3 for $h^* = 0.12$. A second set of parameters corresponding to those originally chosen for 1300 μm DNA (see section 3.3) was also investigated. Also plotted in Figure 3 is the transient fractional stretch for 340 μm DNA again with the same chain discretization as above ($N_{k,s} = 40$ and $N_s = 64$) with $h^* = 0.23$ and $\nu = 0.000\,32$ μm^3. It is clear that this set of parameters also does not quantitatively capture the transient dynamics of 340 μm DNA as compared to experimental results. As in the case of 7-lambda DNA, the parameter set consisting of $h^* = 0.23$ and $\nu = 0.000\,32$ μm^3 leads to transient molecular extension profiles which, on average, show a delayed molecular extension compared to the first set. This observation suggests that as the role of HI becomes more important, the onset of molecular stretch is delayed. However, once any particular molecule begins to stretch, the role of conformation-dependent drag increases for increasing h^*, and molecules may stretch faster. As the length of the polymer molecule increases, we anticipate that consideration of polymer chain resistivity in the *stretched* state will become important for accurate quantitative description of nonequilibrium dynamical behavior as demonstrated by Hsieh et al.,[17] where the hydrodynamic drag on a fully stretched molecule is matched to the Batchelor's drag exerted on a rigid cylindrical body in flow. We have not pursued this further, and such a modification to our simulations is the subject of future study.

We conclude our discussion of relatively short contour length DNA by considering the relaxation of polymer chains from highly strectched conformations. Figure 4 shows the relaxation trajectory of a 7-lambda DNA molecule initially stretched at high flow strengths ($De \gg 15$). The stretch deficit (δ) is defined by the relation
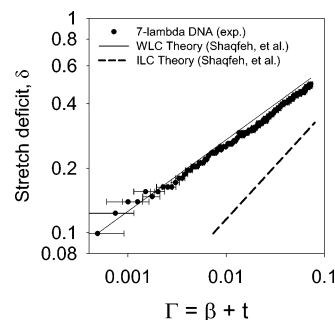

Figure 4. Relaxation of 7-lambda DNA from high stretch. Stretch deficit δ vs dimensionless time Γ from experiment and theory of Shaqfeh et al.[54]

$x = L(1 - \delta)$, where x is the maximum projected stretch of the polymer. We compare the short time relaxtion of DNA from high stretch to recent theory by Shaqfeh et al.[54] This theory uses a single mode (dumbbell) polymer model and invokes asymptotic treatment for the evolution equation for the polymer stress (or, equivalently, the second moment of polymer stretch) within the preaveraging approximation, which is valid for highly stretched polymers. Shaqfeh et al. demonstrate that short time polymer relaxation from any initial stretch deficit δ_0 falls onto a master curve when dimensionless time Γ includes a shift factor β[54] such that $\Gamma = \beta + t$. In this work, time t is made dimensionless with the estimated Rouse relaxation time of the polymer.[55] The shift factor β accounts for the initial stretch deficit δ_0 and may be calculated by the equation

$$\beta = \frac{\delta_0{}^3}{2} \tag{42}$$

The stretch deficit is then given by eq 6 of ref 54

$$\delta = [2\Gamma]^{1/3} \tag{43}$$

Equation 43 shows that at short times polymer relaxation from high stretch follows a power law decay. It should be noted that we extract the longest polymer relaxation time from a single-exponential decay at times much longer than power law behavior is observed. Figure 4 shows good agreement between experiment and theory (solid line).[54] The dotted line shows theoritical stretch deficit for chains obeying an inverse Langevin force law (using Cohen Padé's approximant). Although only one molecular trajectory from the experiment is shown, Figure 4 illustrates typical molecular behavior based on a $\approx$20-molecule DNA ensemble. This work presents the first single molecule experimental observation of DNA relaxation from high stretch with comparison to theory with no adjustable parameters.[54] Error bars in Figure 4 are calculated on the basis of a 5% error in the polymer contour length L.

Conformation-dependent polymer chain resistivities extracted from the multi-bead−spring BD algorithm with fluctuating HI are shown in Figure 5. We plot the normalized resistivity as described in section 3.4 for two values of the flow strength $De = 0.25$ and 0.5. We normalize the dimensionless resistivity ζ for the entire molecule to the Zimm resistivity ζ_0 extracted from coil diffusivities D using the Stokes−Einstein relation $D = kT/\zeta$. Data points are obtained by averaging the external forces described in section 3.4 over long times (at least four polymer relaxation times). For small values of the
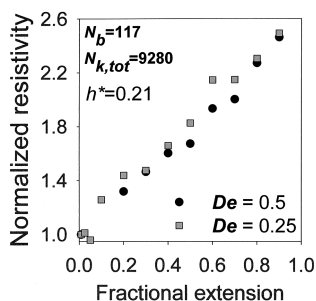
Figure 5. Conformation-dependent resistivity extracted from multi-bead–spring BD simulation with fluctuating HI at De = 0.25 and De = 0.5.

molecular extension, we were able to calculate ζ for low De, where the polymer conformations are not highly perturbed. In this set of simulations, $N = 117$, $N_{k,s} = 80$, $h^* = 0.207$, and $\nu = 0$. Near full extension, the total increase in resistivity from the coiled to stretched state is approximately 2.5. We calculated the ratio of Batchelor drag $\zeta^{stretch}$ on a long, extended cylinder of $L = 1300$ μm (with hydrodynamic radius of 2 nm) *in planar extensional flow* to the Zimm resistivity in the coiled state. Using these molecular parameters in planar extensional flow, the ratio $\zeta^{stretch}/\zeta^{coil}$ is approximately 2.5, and we are satisified by this rough comparison. Finally, we fit a smooth sixth-order polynomial to the resistivity data in Figure 5 and then use this $\zeta(Q)$ functionality in coarse-grained variable drag BD dumbbell simulations (section 3.5) and expressions for ensemble averaged stretch from polymer kinetic theory in section 3.6.

Figure 6 shows the transient molecular extension for DNA with $L = 1300$ μm in planar extensional flow simulated with the BD algorithm with fluctuating HI and EV interactions. Using the model parameters discussed in section 3.3, we simulate single molecule trajectories using a bead–spring chain with $N_s = 123$. At low flow strengths ($De = 0.3$), initialy extended molecules eventually collapse to the coiled conformation over the course of several units of Hencky strain (Figure 6a). As shown in Figure 6b, at $De = 0.48$ slightly below the coil–stretch transition, hysteresis in molecular conformation is apparent as observed in single molecule experiments on 1.3 mm long DNA[29] (see Figure 9 for comparison to experiment). Finally, Figure 6c shows that at flow strengths above the coil–stretch transition ($De = 0.75$) initially coiled molecules eventually unravel to extensions achieved by the initially extended molecules. Molecular stretching is initially slow as interior monomer units become unshielded to the solvent flow field, followed by a rapid stretching of the polymer chain. As noted in section 3.3, we choose the HI and EV parameters for 1.3 mm DNA by matching the experimental relaxation time and steady molecular extension in the coiled polymer state at $De = 0.3$. Polymer conformation hysteresis is also captured in the multi-bead–spring simulations with fluctuating hydrodynamic interactions with other HI and EV parameters. Figure 7a clearly shows conformation hysteresis at $De = 0.48$ for $a = 0.25$ μm ($h^* = 0.207$) and $\nu = 0.0$ for a chain of 117 beads (steady-state polymer extension for this parameter set is shown in Figure 10). Finally, we choose BD simulation parameters $a = 0.20$ μm ($h^* = 0.16$) and $\nu = 0.0$ for a chain consisting of 124 beads. Figure 7b shows the transient polymer extension for this set of parameters at $De = 0.48$, where conformation
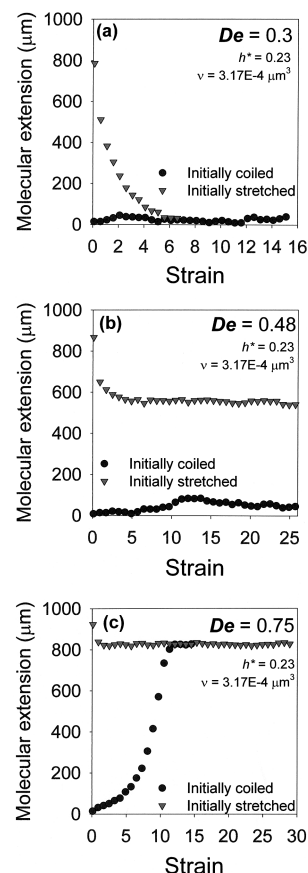

Figure 6. Transient molecular extension for $L = 1300$ μm DNA in planar extensional flow from BD simulation with fluctuating HI and EV interactions at (a) $De = 0.3$, (b) $De = 0.48$, and (c) $De = 0.75$.
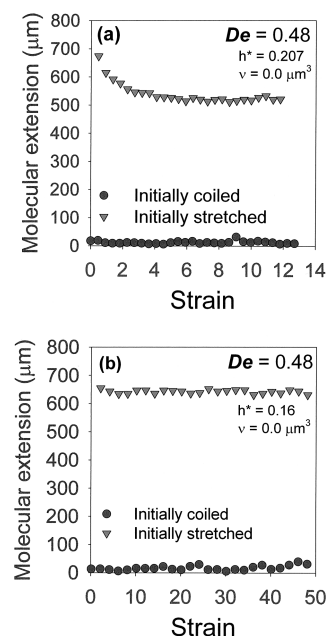

Figure 7. Transient molecular extension for $L = 1300$ μm DNA in planar extensional flow from BD simulation with fluctuating HI (and no excluded volume) at $De = 0.48$ for (a) $h^* = 0.207$ and (b) $h^* = 0.16$.

hysteresis persists up to 50 units of accumulated fluid strain in planar extensional flow.

Next, we were interested in quantitatively comparing results from our multi-bead–spring polymer model with fluctuating HI and excluded-volume interactions to
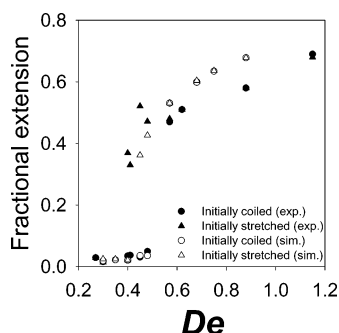
Figure 8. Steady-state fractional molecular extension for $L = 1300$ μm DNA in planar extensional flow from recent experimental data given by Schroeder et al.[29] and from BD simulation with fluctuating HI and EV interactions ($h^* = 0.23$ and $\nu = 0.000\,32$ μm^3).
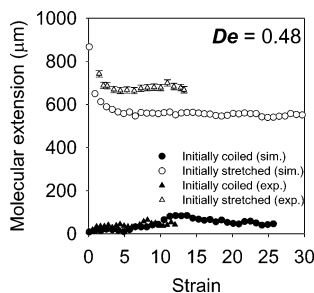

Figure 9. Transient molecular extension in planar extensional flow for $L = 1300$ μm DNA from recent experimental data given by Schroeder et al.[29] and from BD simulation with fluctuating HI and EV interactions ($h^* = 0.23$ and $\nu = 0.000\,32$ μm^3).

recent single molecule experiments on 1.3 mm DNA in planar extensional flow by Schroeder et al.[29] Figure 8 shows the steady state fractional molecular extension for DNA molecules approximately 1300 μm in length from experiment and 1300 μm DNA from BD simulations ($h^* = 0.23$ and $\nu = 0.000\,32$ μm^3). The simulation quantitatively captures experimental behavior at $De = 0.3$ and shows conformation hysteresis in the general range of De as in experiments, giving reasonably accurate results in the hysteresis region for initially coiled and stretched molecules. Simulated steady fractional extension at $De = 0.57$ and above does not exhibit conformation hysteresis as observed in single molecule experiments. Simulated polymer extension at $De = 0.75$ is approximately 10% larger than experimental results. It should be noted that the experimental data represents steady molecular extension for molecules approximately 1300 μm in length, as it was difficult to obtain monodisperse DNA molecules with large contour lengths, so rigorous comparison with BD simulation is difficult. Finally, Figure 9 compares transient molecular extension in planar extensional flow from experiment and BD simulation at $De = 0.48$. Simulation accurately captures initially coiled polymer behavior, though it underpredicts DNA extension in the initially extended state at $De = 0.48$. Again, polydispersity in the experimental DNA samples may be one reason for the discrepancy, as the BD simulations are not consistently over- or underpredicting steady-state fractional molecule extension as compared to experimental values.

We also investigated coarse-grained dumbbell polymer models with conformation-dependent resistivities. Using the Brownian dynamics algorithm described in section 3.5, we employ the smooth polynomial fit to the $\zeta(Q)$ data shown in Figure 5 to simulate both transient
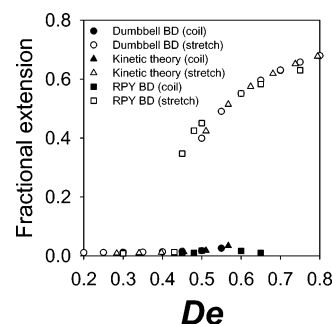

Figure 10. Steady-state fractional molecular extension for multi-bead–spring polymer molecules with fluctuating HI ($h^* = 0.207$) and ensemble averaged steady extension from variable drag Brownian dumbbell simulations and from polymer kinetic theory using a conformation-dependent resistivity for both initially coiled and extended polymer dumbbells.

and steady-state molecular extensions in planar extensional flow. Figure 10 shows steady fractional molecular extension extracted from long time averages (or large accumulated Hencky strains, $\epsilon \geq 50$) for ensembles of 250 dumbbells. We also plot the ensemble average steady-state molecular stretch $\langle R_i R_i \rangle^{1/2}/L$ from kinetic theory using $\zeta(R)$ as described in section 3.6. Steady $\langle R_i R_i \rangle^{1/2}/L$ from theory and BD simulations are calculated by initializing the dumbbells in either a randomly coiled or highly extended (80% L along the principal axis of stretch direction) conformation. Here, the dimensionless flow strength De is defined using the longest polymer relaxation time from the variable drag dumbbell simulations for both BD and kinetic theory results. A sizable region of conformation hysteresis near the coil–stretch transition is apparent, similar to the steady-state molecular stretch shown in Figure 6 from the multi-bead–spring BD model with fluctuating HI.

Figure 10 also shows the steady fractional molecular extension from the multi-bead–spring BD simulation with fluctuating HI ($h^* = 0.207$). This plot demonstrates that results from the coarse-grained BD dumbbell simulations and kinetic theory with variable drag provide remarkably accurate steady-state results in planar extensional flow when compared to the multi-bead–spring BD simulation. Initially coiled data points from the multibead simulation at $De = 0.6$ and $De = 0.65$ were taken over 20 and 15 units of Hencky strain, respectively; these data points deviate from the coarse-grained simulations, though given larger strain averages, molecules at these flow strengths may eventually unravel to the extended state. Individual trajectories from dumbbell BD simulations for initially coiled molecules near $De \approx 0.5$ show that polymers are slow to unravel, and data points at $De = 0.55$ and 0.6 are calculated from long time transient extension averages ($\epsilon \geq 250$). The hysteresis window for the multi-bead–spring chain BD simulations in Figure 10 (without excluded-volume interactions) is wider than the hysteresis region shown in Figure 8 for multi-bead–spring chains with excluded volume. Presumably, bead overlap in the case of polymer chains without EV causes more hydrodynamic shielding in the coiled polymer state.

As discussed in previous work,[29] the ensemble averaged steady-state molecular extension should be single-valued (although the probability distribution ψ may be double-peaked). Our experiments and simulations occur over finite times during which initially coiled or initially stretched polymers are trapped in effective energy minima. Effective barrier heights (shown in Figure 12)
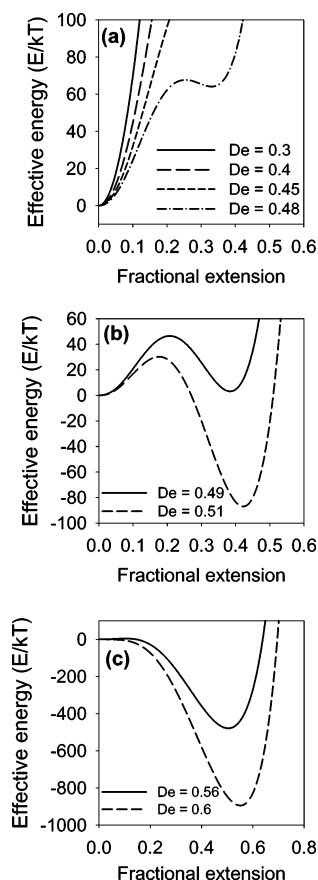
Figure 11. Effective conformational polymer energies in planar extensional flow calculated using kinetic theory for a dumbbell with variable resistivity.

are much greater than thermal energy, and therefore an initially coiled (or conversely, initially stretched) molecule will remain trapped in its conformation over the course of the experiment or simulation. If observation of molecular extension for effectively infinite times is possible, one may observe the system evolve to the lowest energy (highest probability) state of conformation. For the finite time simulations shown in Figure 10, however, the steady-state molecular extension will be multivalued in the hysteresis region for most realistic situations if the polymer is larger than a critical length.

Finally, we calculate the effective conformational energy given by eq 41 at a few values of the flow strength De, and these are plotted in Figure 11a−c. At low flow strengths ($De \leq 0.48$), the effective energy has a single minimum corresponding to the coiled polymer state, and the steady-state molecular extension plot is single-valued as shown in Figure 10. However, for slightly larger flow strengths near the coil−stretch transition, the effective conformational energy is double-welled as shown in Figure 11, and the polymer conformation hysteresis is observed. As a result, the steady-state polymer extension is multivalued as shown in Figure 10. Finally, for higher flow strengths, again a single minumum in the effective conformation energy occurs representing the extended polymer state. The effective conformational energy barrier heights are plotted in Figure 12a,b. Figure 12a shows that the barrier heights are extremely large ($\gg kT$) for initially coiled polymers for De near the onset of hysteresis and conversely for initially stretched polymers at high De in the hysteresis window. It is clear that "state hopping"
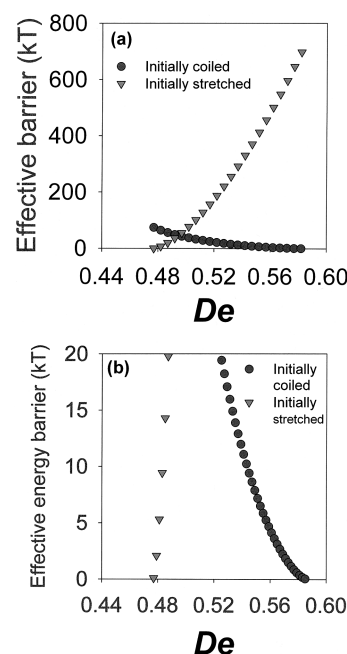

Figure 12. Effective energy barrier heights for initially coiled and initially stretched molecules calculated using polymer kinetic theory for a dumbbell with variable resistivity.

will not occur here given the magnitude of these barrier heights. Furthermore, Figure 12b shows that the barrier heights rise sharply for initially stretched molecules near the onset of hysteresis (at low De) and conversely for initially coiled molecules near the largest De value at which conformation hysteresis occurs. The magnitude of the effective barrier heights is much greater than thermal energy, and the sole influence of Brownian motion was not strong enough to cause an initially coiled (stretched) polymer to visit the stretched (coiled) state in the range of De where conformation hysteresis was observed. Therefore, we do not anticipate (and we did not observe) state hopping between the coiled and stretched polymer states for 1.3 mm DNA in the range of flow strengths that give conformation hysteresis for planar extensional flow.

5. Conclusion

Using a combination of single molecule visualization and Brownian dynamics techniques, we are able to characterize the influence in intramolecular hydrodynamic interactions on polymer chain dynamics for large DNA molecules. Quantitative agreement between transient molecular extension in experiment and BD simulation with fluctuating HI and EV interactions is achieved for DNA with $L \approx 150 \ \mu$m. Polymer conformation hysteresis is simulated for large DNA chains (1.3 mm in length) with reasonably accurate quantitative experimental agreement when the HI and EV model parameters are chosen to match the experimental relaxation time and dynamical polymer stretch at low flow strengths in extensional flow. Finally, we demonstrate that the conformation-dependent resistivity of large chains extracted from the multi-bead−spring with fluctuating HI may be used to predict polymer behavior in simple coarse-grained polymer models in planar extensional flow. In particular, conformation hysteresis is accurately predicted in the coil−stretch transition in planar extensional flow, as shown in the steady-state polymer extension calculated from variable drag dumb-

bell Brownian dynamics simulation and from polymer kinetic theory for a dumbbell with variable resistivity.

References and Notes

(1) Fuller, G. G.; Leal, L. G. *Rheol. Acta* **1980**, *19*, 580.
(2) Dunlap, P. N.; Leal, L. G. *J. Non-Newtonian Fluid Mech.* **1987**, *23*, 5.
(3) Hunkeler, D.; Nguyen, T. Q.; Kausch, H. H. *Polymer* **1996**, *37*, 4257.
(4) Menasveta, M. J.; Hoagland, D. A. *Macromolecules* **1991**, *24*, 3427.
(5) Lee, E. C.; Muller, S. J. *Macromolecules* **1999**, *32*, 3295.
(6) Smith, D. E.; Babcock, H. P.; Chu, S. *Science* **1999**, *283*, 1724.
(7) Perkins, T. T.; Smith, D. E.; Chu, S. *Science* **1997**, *276*, 2016.
(8) Smith, D. E.; Chu, S. *Science* **1998**, *281*, 1335.
(9) Babcock, H. P.; Teixeira, R. E.; Hur, J. S.; Shaqfeh, E. S. G.; Chu, S. *Macromolecules* **2003**, *36*, 4544.
(10) Perkins, T. T.; Smith, D. E.; Larson, R. G.; Chu, S. *Science* **1995**, *268*, 83.
(11) Smith, D. E.; Perkins, T. T.; Chu, S. *Macromolecules* **1996**, *29*, 1372.
(12) Larson, R. G.; Hu, H.; Smith, D. E.; Chu, S. *J. Rheol.* **1999**, *43*, 267.
(13) Hur, J. S.; Shaqfeh, E. S. G.; Larson, R. G. *J. Rheol.* **2000**, *44*, 713.
(14) Hur, J. S.; Shaqfeh, E. S. G.; Babcock, H. P.; Smith, D. E.; Chu, S. *J. Rheol.* **2001**, *45*, 421.
(15) Öttinger, H. C. *Stochastic Processes in Polymeric Fluids*; Springer: Berlin, 1996.
(16) Larson, R. G. *The Structure and Rheology of Complex Fluids*; Oxford University Press: New York, 1999.
(17) Hsieh, C. C.; Li, L.; Larson, R. G. *J. Non-Newtonian Fluid Mech.* **2003**, *113*, 147.
(18) Cifre, J. G. H.; de la Torre, J. G. *J. Rheol.* **1999**, *43*, 339.
(19) Cifre, J. G. H.; de la Torre, J. G. *J. Chem. Phys.* **2001**, *115*, 9578.
(20) Neelov, I. M.; Adolf, D. B.; Lyulin, A. V.; Davies, G. R. *J. Chem. Phys.* **2002**, *117*, 4030.
(21) Neelov, I. M.; Adolf, D. B. *Macromolecules* **2003**, *36*, 6914.
(22) Zimm, B. H. *J. Chem. Phys.* **1956**, *24*, 269.
(23) Öttinger, H. C. *J. Chem. Phys.* **1987**, *86*, 3731.
(24) Zylka, W.; Öttinger, H. C. *J. Chem. Phys.* **1988**, *90*, 474.
(25) Öttinger, H. C. *J. Chem. Phys.* **1988**, *90*, 463.
(26) Wedgewood, L. E. *J. Non-Newtonian Fluid Mech.* **1989**, *31*, 127.
(27) Jendrejack, R. M.; de Pablo, J. J.; Graham, M. D. *J. Chem. Phys.* **2002**, *116*, 7752.
(28) Quake, S. R.; Babcock, H. B.; Chu, S. *Nature (London)* **1997**, *388*, 151.
(29) Schroeder, C. M.; Babcock, H. P.; Shaqfeh, E. S. G.; Chu, S. *Science* **2003**, *301*, 1515.
(30) Tanner, R. I. *Trans. Soc. Rheol.* **1975**, *19*, 557.
(31) Lumley, J. *J. Polym. Sci., Macromol. Rev.* **1973**, *7*, 263.
(32) Schroeder, C. M.; Babcock, H. B.; Shaqfeh, E. S. G.; Chu, S. U.S. Provisional Patent Application No. 60/498,875, 2003.
(33) Ermak, D. L.; McCammon, J. A. *J. Chem. Phys.* **1978**, *69*, 1352.
(34) Bird, R. B.; Curtiss, C. F.; Armstrong, R. C.; Hassager, O. *Dynamics of Polymeric Liquids*, 2nd ed.; Wiley: New York, 1987; Vol. 2.
(35) Russel, W. B.; Saville, D. A.; Schowalter, W. R. *Colloidal Dispersions*; Cambridge: New York, 1989.
(36) Rotne, J.; Prager, S. *J. Chem. Phys.* **1969**, *50*, 4831.
(37) Somasi, M.; Khomami, B.; Woo, N. J.; Hur, J. S.; Shaqfeh, E. S. G. *J. Non-Newtonian Fluid Mech.* **2002**, *108*, 227.
(38) Marko, J. F.; Siggia, E. D. *Macromolecules* **1995**, *28*, 8759.
(39) Doi, M.; Edwards, S. F. *The Theory of Polymer Dynamics*; Clarendon: Oxford, 1986.
(40) Prakash, J. R. *J. Rheol.* **2002**, *46*, 1353.
(41) Prakash, J. R.; Öttinger, H. C. *Macromolecules* **1999**, *32*, 2028.
(42) Prakash, J. R. *Macromolecules* **2001**, *34*, 3396.
(43) Graessley, W. W.; Hayward, R. C.; Grest, G. S. **1999**, *32*, 3510.
(44) Kreyszig, E. *Advanced Engineering Mathematics*, 7th ed.; Wiley: New York, 1993.
(45) Jendrejack, R. M.; Graham, M. D.; de Pablo, J. J. *J. Chem. Phys.* **2000**, *113*, 2894.
(46) Fixman, M. *Macromolecules* **1986**, *19*, 1204.
(47) Batchelor, G. K. *J. Fluid Mech.* **1970**, *44*, 419.
(48) Grassia, P. S.; Hinch, E. J.; Nitsche, L. C. *J. Fluid Mech.* **1995**, *282*, 373.
(49) Fixman, M. *J. Chem. Phys.* **1978**, *69*, 1527.
(50) Hinch, E. J. *Proc. Coll. Int. CNRS Polym. Lubrification* **1974**, *233*, 241.
(51) De Gennes, P. G. *J. Chem. Phys.* **1974**, *60*, 5030.
(52) Fan, X. J.; Bird, R. B.; Renardy, M. *J. Non-Newtonian Fluid Mech.* **1985**, *18*, 255.
(53) Stevenson, J. F.; Bird, R. B. *Trans. Soc. Rheol.* **1971**, *15*, 135.
(54) Shaqfeh, E. S. G.; McKinley, G. H.; Woo, N.; Nguyen, D. A.; Sridhar, T. *J. Rheol.* **2004**, *48*, 209.
(55) Li, L.; Larson, R. G.; Sridhar, T. *J. Rheol.* **2001**, *44*, 291.

MA049461L